Full Text View

Volume 30, Issue 9 (September 2000)

Journal of Physical Oceanography
Article: pp. 2231–2245 | Abstract | PDF (271K)

Double-Diffusive Interleaving in the Presence of Turbulence: The Effect of a Nonconstant Flux Ratio

David Walsh

International Arctic Research Center, University of Alaska, Fairbanks, Fairbanks, Alaska

Barry Ruddick

Department of Oceanography, Dalhousie University, Halifax, Nova Scotia, Canada

(Manuscript received May 17, 1999, in final form October 11, 1999)

DOI: 10.1175/1520-0485(2000)030<2231:DDIITP>2.0.CO;2

ABSTRACT

The influence of turbulent mixing on double-diffusively driven thermohaline interleaving is investigated. The problem is formulated using a turbulence-modified flux ratio to link the fluxes of T and S; the addition of turbulence changes the way in which the effective flux ratio varies with the density ratio R_ρ. Formulation of the problem maps onto past interleaving studies, except that the flux ratio is a function of R_ρ in the present work. Posing the problem in this way allows the effects of turbulence and intrinsic variations in the salt-finger flux ratio to be studied within the same theoretical framework.

Turbulence modifies the slope, wavelength, and growth rate of the fastest-growing intrusions, decreasing the range of slopes and wavenumbers that can grow. However, analysis shows that growing solutions exist for any finite value of the turbulent diffusivity K^t, suggesting that double-diffusively driven intrusions can exist in the ocean even when double-diffusive fluxes are much weaker than turbulent fluxes.

If the flux ratio is a decreasing function of R_ρ (as suggested by some models of salt finger convection) a different instability occurs, which has unbounded growth rates in the high wavenumber limit (a “UV catastrophe”). In most cases, the instability can be suppressed by the addition of sufficiently strong turbulent mixing. The threshold for this instability depends upon variation of the T/S flux ratio with R_ρ, and hence on the relative strengths of turbulent and double-diffusive mixing. The instability is shown to be nonintrusive in nature, as it does not rely upon lateral advection across a front; it is found to be closely related to the one-dimensional double-diffusive instability investigated by Huppert.

1. Introduction

Thermohaline interleaving is often observed in regions of the ocean characterized by strong lateral T–S gradients. Interleaving was first documented by Hamon (1967) and Stommel and Fedorov (1967), who recognized that it could be an important mechanism for cross-front mixing. Since then, interleaving has been documented on the edges of mesoscale

eddies (Ruddick 1992), on the periphery of major currents (Toole 1981), on shelf-break fronts (Horne 1978; Barton and Hughes 1982), and generally at confluences of water masses with differing T–S properties. Carmack et al. (1998) observed interleaving layers of Atlantic and Pacific water in the Arctic Ocean; these layers (or intrusions) were laterally coherent over distances of more than 1000 km. Carmack et al. suggested they may play an important role in recent large-scale thermohaline transitions within the Arctic Ocean. Richards and Pollard (1991) suggest that intrusions several hundred kilometers long in the near-surface waters of the equatorial Pacific might be associated with strong lateral mixing within the thermocline.

Stern (1967) identified salt finger convection as a possible driving mechanism for interleaving, but the lack of friction in his theoretical model led to unbounded growth rates in the high wavenumber limit. This was remedied by Toole and Georgi (1981), who incorporated friction into Stern's model. Their modification led to a prediction of a finite wavelength for the fastest-growing intrusion, in reasonably good agreement with observations. Since Toole and Georgi's study, numerous theoretical studies have appeared, most of which are variations on their linearized stability analysis. Holyer (1983) investigated intrusions driven by molecular fluxes of T and S and found that growth was possible, even when the stratification was stable to double-diffusive convection, because the molecular diffusivities of T and S differ. McDougall (1985a) recast Toole and Georgi's analysis in a layer framework, assuming a background of convecting layers separated by double-diffusive interfaces. Walsh and Ruddick (1995a) investigated the effect of R_ρ-dependent diffusivities on growing intrusions and found that nonconstant diffusivities could lead to growth rates much larger than predicted by constant diffusivity models. Kuz'mina and Rodionov (1992) and May and Kelley (1997) have examined the effect of baroclinic shear on intrusions, and their work suggests that background shear can have an important effect on growing intrusions. May and Kelley argue that shear may either increase or decrease growth rates, depending on the relative signs of the cross-front salinity and density gradients.

Most theoretical investigations since Stern's (1967) study have assumed that small-scale fluxes are purely double diffusive. However, while stratification conditions in large parts of the World Ocean are unstable to salt fingering (Schmitt 1981), salt fingers rarely occur without turbulence. Except perhaps in large-scale thermohaline staircases like the C-SALT staircase (Schmitt et al. 1987), both fingers and turbulence typically contribute to the total flux of salt, heat, and buoyancy. Microstructure observations by Ruddick et al. (1997) in the North Atlantic Tracer Release Experiment (NATRE) used the "scaled diffusivity ratio," Γ_d, to diagnose double-diffusive effects and failed to find significant evidence of salt finger enhancement of turbulent fluxes. Due to lower noise levels and the ability to observe the Richardson number directly, St. Laurent and Schmitt (1999) found that the observed Γ_d in the NATRE region was consistent with salt fingers for segments with Richardson number greater than one, low values of R_ρ, and high χ (to address signal/noise issues only the highest 25% of χ values were used in their analysis). Segments with Richardson number less than one, or with double-diffusively stable (i.e., nonfingering) stratification had Γ_d consistent with turbulence values. This indicates the conditions under which salt fingers may be found in central waters: absence of turbulence and low R_ρ, and makes it clear that salt fingers and turbulence coexist in such regions. St. Laurent and Schmitt formulated a model of coexisting, noninteracting turbulence and salt fingers in which the effects are additive and estimated the net fluxes in the NATRE region. The salt diffusivity was found to be enhanced by 60% over the thermal diffusivity estimated from the Osborn–Cox (1972) model. Good agreement was found between the salt diffusivity and the directly observed tracer diffusivity, and the buoyancy flux divergence was computed, leading to an estimated diapycnal velocity of ≈ -1.7 m yr^{-1}, which compared favorably to that inferred from the tracer. Thus, the analysis of St. Laurent and Schmitt demonstrates that, in the NATRE region, diapycnal mixing of heat, salt, and tracers is dominated by turbulence but enhanced by salt fingers. By focusing on data segments with large Richardson number and large χ, St. Laurent and Schmitt found evidence that the T/S flux ratio in the NATRE region was a decreasing function of the density ratio R_ρ, in qualitative agreement with the salt finger model due to Stern (1975). While this result is suggestive, interpretation is difficult because the effect of turbulence on the net flux ratio and on the effective diffusivity for density is critically dependent on the relative balance between turbulence and salt fingers and on how that balance depends on the density ratio and Richardson number.

Even if turbulent fluxes dominate over double-diffusive fluxes in many situations, evidence still points to double diffusion as a primary driving mechanism for interleaving. Convincing evidence for this was provided by Ruddick (1992), who showed that intrusion slopes and wavelengths in Meddy Sharon were consistent with double-diffusive driving, both in the upper (diffusively stratified) and lower (salt finger stratified) halves of the meddy. Ruddick inferred an effective salt diffusivity of $K_S \approx 3 \times 10^{-5}$ m^2 s^{-1} in the interleaving layers, comparable with the value of 1–2 ($\times 10^{-5}$ m^2 s^{-1}) typical of shear-driven mixing in the thermocline (e.g., Ledwell et al. 1993). Given the ubiquitous nature of turbulence in the ocean, it is likely that both double diffusion and turbulence were present within these intrusions, and this raises the question of how intrusions are affected by turbulence. In order to assess the importance of intrusive fluxes in the ocean, a better understanding is needed of the factors that limit their growth at large amplitude and set fluxes. One such factor is turbulence, which can alter the balance between buoyancy-driven cross-front advection and friction.

In this work, we extend that of Walsh and Ruddick (1995a) by incorporating the effects of high Reynolds number turbulent mixing. In addition, we explore the consequences of using a more realistic R_ρ-dependent formulation for the salt finger flux ratio &lsqb≤ke those proposed by Stern (1975, pp. 192–195) and Schmitt (1979a)], rather than the constant value used in most previous theoretical studies of interleaving. The problem is formulated so that turbulence appears as an R_ρ-dependent T/S flux ratio. This allows an examination of the effects of both turbulence and nonconstant finger flux ratio within the same theoretical framework.

In section 2 we formulate the model equations, then linearize the equations and derive a growth rate polynomial for the linearized system. In section 3, we consider the constant finger flux ratio case and show that the addition of turbulence damps out high-wavenumber intrusions that would otherwise grow. Next, we demonstrate that the qualitative character of the solutions can be inferred from properties of the marginal stability curve. The marginal stability curve is found to be either

elliptical or hyperbolic when plotted as a function of the slope s and squared vertical wavenumber m^2, a result independent of the detailed form of the diffusivity and flux ratio formulations used. In section 4, we consider the effect of a nonconstant salt finger flux ratio and show that using either the formulation due to Stern (1975) or that due to Schmitt (1979a) leads to a high wavenumber "UV" instability different from the classical intrusive instability, but qualitatively similar to that discussed by Huppert (1971). Finally, we demonstrate that the qualitative properties of the solutions depend only on variation of the turbulence-modified flux ratio with R_ρ. We end with a discussion (section 5) and conclusions (section 6).

2. The model

Our approach is similar to that of Walsh and Ruddick (1995a). We investigate the linear stability of a "front" characterized by uniform horizontal and vertical gradients of temperature and salinity. The basic state is assumed to be unstable to salt finger convection, so $\alpha\overline{T}_z > \beta\overline{S}_z$. Figure 1 shows quasi-lateral interleaving layers on a wide front, with warm and salty layers rising and cool and fresh layers descending as they cross the front. Vertical profiles of salinity, temperature, and the associated buoyancy fluxes (shown as vectors) taken at "A" are also shown. For the case shown, vertical buoyancy flux convergences due to salt fingering reinforce the initial motion, causing the intrusions to accelerate across the front. The difference between this study and Walsh and Ruddick (1995a) is in the parameterization of the small-scale vertical fluxes, which here are taken to be due to a linear superposition of turbulence and double diffusion rather than pure double diffusion. Following Walsh and Ruddick (1995a), the model equations are

$$u_t + p_x/\rho_0 = -F_z^{(u)} \qquad (1a)$$

$$w_t + p_z/\rho_0 + g(\beta S - \alpha T) = -F_z^{(w)} \qquad (1b)$$

$$u_x + w_z = 0 \qquad (1c)$$

$$S_t + u\overline{S}_x + w\overline{S}_z = -F_z^{(S)} \qquad (1d)$$

$$T_t + u\overline{T}_x + w\overline{T}_z = -F_z^{(T)}. \qquad (1e)$$

The $F^{(\cdot)}{}_z$ terms represent vertical flux divergences of heat, salt, and momentum. Incorporated in (1) is the assumption that intrusions have small slopes, and therefore horizontal flux divergences are negligible compared with vertical flux divergences. Equations (1a–c) can be simplified by using the streamfunction ψ, defined as

$$\psi_x = w \qquad \psi_z = -u, \qquad (2)$$

in which case (1a–c) reduce to a single equation for the alongfront vorticity $\nabla^2\psi$:

$$\nabla^2\psi_t + g(\beta S_x - \alpha T_x) = F^{(u)}{}_{zz} - F^{(w)}{}_{zx}, \qquad (3)$$

indicating that the alongfront vorticity changes in response to cross-front variations in anomalous density and diffusion effects.

Small-scale vertical fluxes of heat, salt, and momentum are specified using eddy diffusivities and viscosities, with finger fluxes of heat and salt linked via the finger flux ratio γ_f

$$\alpha F^{(T)}{}_{\text{fingers}} = \gamma_f \beta F^{(S)}{}_{\text{fingers}}, \qquad (4)$$

as first suggested by Stern (1967). As in Walsh and Ruddick (1995a), diffusivities and viscosities are taken to be functions of the density ratio R_ρ:

$$R_\rho = \frac{\alpha T_z}{\beta S_z}. \qquad (5)$$

The fluxes in (1) are thus given by

$$F^{(u)} = -Au_z = -[A^f(R_\rho) + A^t]u_z \qquad (6a)$$

$$F^{(w)} = -Aw_z = -[A^f(R_\rho) + A^t]w_z \qquad (6b)$$

$$F^{(S)} = -K_S S_z = -[K_S^f(R_\rho) + K^t]S_z \qquad (6c)$$

$$F^{(T)} = -K_T T_z = -\left(\gamma_f(R_\rho)\frac{K_S^f(R_\rho)}{R_\rho} + K^t\right)T_z, \qquad (6d)$$

where in (6d) Eq. (4) has been used to express finger fluxes of temperature in terms of the salt flux. The superscripts "f" and "t" in (6) denote salt fingers and turbulence, respectively, so K^f_S is a finger diffusivity and K^t a turbulent diffusivity. We

take the turbulent diffusivities of T and S to be equal, consistent with the idea that turbulent mixing is caused by energetic high-Reynolds-number turbulence. Flux laws like (6) have been used by Kuz'mina and Rodionov (1992) in an investigation focusing on the effect of baroclinicity on double-diffusive interleaving.

A number of studies have addressed the coexistence of fingers and turbulence. McDougall and Ruddick (1992) proposed a method of interpreting microstructure data that can in principle differentiate between double diffusion and shear-driven turbulent mixing. Their theory is based on the assumption that salt fingers and turbulence have very different timescales, so their combination can be approximately represented by a linear combination of finger and turbulent fluxes. These ideas are consistent with laboratory studies due to Crapper (1976) and Linden (1971), who also suggest that turbulent and finger fluxes add linearly.

In most theoretical studies of interleaving, the salt finger flux ratio γ_f is taken to be constant, with a value in the range of 0.5–0.9. However, theoretical models of of salt fingers (Stern 1975) and laboratory experiments (Schmitt 1979b) indicate that γ_f is a decreasing function of R_ρ, with a maximum value at $R_\rho = 1$. A more complete analysis by Schmitt (1979a) indicates that γ_f is a decreasing function of R_ρ for relatively small values of R_ρ, but may be an increasing function of R_ρ for large R_ρ ($R_\rho \gtrsim 4$). For the diffusive case, Kelley (1984) has analyzed staircase data that indicate the diffusive flux ratio γ_d is largest when $R_\rho = 1$ and decreases monotonically away from $R_\rho = 1$.

The functional forms of K^f_S and A^f are poorly known. Schmitt's (1981) study suggests that K^f_S is maximum near $R_\rho = 1$ (where finger growth rates are largest) and decreases rapidly with increasing R_ρ. Kunze (1994) proposed a model for salt fingers disrupted by intermittent turbulence. Kunze's results suggest that K^f_S may increase with R_ρ for small values of R_ρ but should decrease with R_ρ for larger R_ρ, in agreement with Schmitt's result. There are further discrepancies between the diffusivities predicted by Schmitt and Kunze, the most notable being that Schmitt's diffusivities are some two orders of magnitude larger than those predicted by Kunze and are almost certainly too large. In the following derivation we will carry through the full R_ρ dependence of the diffusivity and viscosity for the sake of completeness but, in the discussion sections that follow, we will focus almost exclusively on the effect of an R_ρ-dependent flux ratio rather than on the effect of a nonconstant diffusivity. This is due to the uncertain diffusivities, and because the effect of R_ρ-dependent diffusivity on interleaving has already been discussed by Walsh and Ruddick (1995a,b).

Equations (6c,d) can be manipulated to give

$$\alpha F^{(T)} = \left(\frac{\gamma_f K^f_S + K^t R_\rho}{K^f_S + K^t} \right) \beta F^{(S)}. \qquad (7)$$

Comparing (7) with (4) shows that the expression in parentheses in (7) has the form of a turbulence-modified "effective" T/S flux ratio

$$\gamma_{\text{eff}}(R_\rho) \equiv \frac{\gamma_f(R_\rho) K^f_S(R_\rho) + R_\rho K^t}{K^f_S(R_\rho) + K^t}. \qquad (8)$$

The effective flux ratio γ_{eff} is a function of R_ρ even when both γ_f and K^f_S are constants. For nonzero K^t/K^f_S and constant γ_f (=0.6), γ_{eff} is a monotonically increasing function of R_ρ (Fig. 2).

Using (1d), (1e), (3), (6), and (8), the governing equations can be written in the form:

$$\begin{aligned} \nabla^2 \psi_t + g(\beta S_x - \alpha T_x) &= (A(R_\rho)\psi_{xz})_{xz} + (A(R_\rho)\psi_{zz})_{zz} \\ S_t + u\bar{S}_x + w\bar{S}_z &= (K_S(R_\rho)S_z)_z \\ T_t + u\bar{T}_x + w\bar{T}_z &= \left(\gamma_{\text{eff}} \frac{\beta}{\alpha} K_S(R_\rho) S_z \right)_z . \end{aligned} \qquad (9)$$

These are identical to the equations analyzed by Walsh and Ruddick (1995a), except that the finger flux ratio has been replaced by the modified flux ratio γ_{eff}, which is a function of R_ρ (and hence is differentiated). Putting $S = \bar{S} + \tilde{S}$, $T = \bar{T} + \tilde{T}$, $\psi = \tilde{\psi}$ in (9) [where terms with tildes (;tz·) are small perturbations], defining $\bar{R}_\rho = \alpha \bar{T}_z / \beta \bar{S}_z$, and keeping only terms linear in perturbation quantities gives the linearized version of (9):

Primes denote differentiation with respect to R_ρ, and diffusivities and viscosities in (10) are evaluated at $R_\rho = \overline{R}_\rho$. While the effects of turbulent mixing are incorporated into the right-hand sides of (10a–c), the purely double-diffusive case may be recovered by setting $\gamma_{\text{eff}} = \gamma_f$, $A = A^f$, and $K_S = K^f_S$.

Except for the horizontal braced terms, (10) is identical to the equations analyzed by Walsh and Ruddick (1995a) with γ_f replaced by γ_{eff}. Variations in the viscosity do not enter into the problem at this order, as discussed in Walsh and Ruddick (1995a). Further, although (10) does not include rotational effects, Toole and Georgi (1981) and McDougall (1985a) have shown that, in the absence of large-scale shear, the vertical wavenumber, cross-front slope, and growth rate of the fastest-growing intrusions are unaffected by rotation. The main effect of rotation is to induce an alongfront tilt such that cross-frontal velocities are in thermal-wind balance. Finally, in deriving (10) it is assumed that $\overline{\rho}_x = 0$ (i.e., $\alpha\overline{T}_x = \beta\overline{S}_x$), so the fluid is motionless in the basic state. In the rotating case, this assumption removes the complication of alongfront geostrophic shear, which will tilt intrusions and disrupt their growth, a possibility which led May and Kelley (1997) to suggest that intrusions in strongly sheared fronts cannot tilt in the alongfront direction.

The growth rate polynomial for (10) is obtained by substituting solutions of the form $e^{i(k;zzx+m;zzz)+\lambda;zzt}$ into the linearized form of (10), giving

$$\lambda^3 + \lambda^2 m^2[1 + \text{Pr} + (\gamma_{\text{eff}} - \overline{R}_\rho)K'_S/K_S + \underbrace{\gamma'_{\text{eff}}}] + \lambda(\text{Pr}m^4[1 + (\gamma_{\text{eff}} - \overline{R}_\rho)K'_S/K_S + \underbrace{\gamma'_{\text{eff}}}] + s^2) + \underbrace{\gamma'_{\text{eff}}\,\text{Pr}m^6}$$
$$- [1 + (1 - \overline{R}_\rho)K'_S/K_S]m^2 s(\varepsilon_x - s(1 + \varepsilon_z)) - \underbrace{\gamma'_{\text{eff}} s m^2(\varepsilon_x - s\varepsilon_z)/\varepsilon_z} = 0. \qquad (11)$$

(Click the equation graphic to enlarge/reduce size)

The following dimensionless quantities have been introduced:

$$\begin{aligned}
\lambda &= \lambda_*/\overline{N} && \text{(growth rate)}\\
m &= m_*\sqrt{K_S/\overline{N}} && \text{(vertical wavenumber)}\\
s &= k_*/m_* && \text{(cross-front slope)}\\
\text{Pr} &= A/K_S && \text{(Prandtl number)}\\
\mathcal{S}_x &= g\beta\overline{S}_x/\overline{N}^2 && \text{(horizontal salinity gradient)}\\
\mathcal{S}_z &= g\beta\overline{S}_z/\overline{N}^2 &&\\
&= 1/(\overline{R}_\rho - 1) && \text{(vertical salinity gradient)}\\
\varepsilon_x &= (1 - \gamma_{\text{eff}})\mathcal{S}_x &&\\
\varepsilon_z &= (1 - \gamma_{\text{eff}})\mathcal{S}_z = (1 - \gamma_{\text{eff}})/(\overline{R}_\rho - 1). && (12)
\end{aligned}$$

We have assumed that intrusion slopes are small ($s \ll 1$) in deriving (11). Expression (11) generalizes Eq. (13) from Walsh and Ruddick (1995a) to include a nonconstant flux ratio; horizontal braced terms in (11) did not appear in the growth rate polynomial analyzed by Walsh and Ruddick (1995a). The polynomial (11) was discussed briefly by Walsh and Ruddick (1998), who used it to initialize their numerical model, although they did not discuss its properties in detail.

We will show that (11) admits two different instabilities: the standard intrusive instability analyzed by Toole and Georgi (1981), which has peak growth rates at a finite value of the vertical wavenumber m, and an instability with unbounded growth rates in the large m limit (henceforth referred to as the high-wavenumber or "UV" instability), which occurs when the flux ratio γ_{eff} is a decreasing function of R_ρ. The two instabilities can coexist, and in general intrusions dominate for smaller values of m, while the UV instability dominates at large m.

a. The marginal stability curve

Information about intrusion growth rates, slopes, wavenumbers, and parameter dependencies can be gained by considering the marginal stability properties of (11). Setting $\lambda = 0$ in (11) gives the condition for marginal stability:

$$m^2\{\gamma'_{\text{eff}}\,\text{Pr}m^4 - [1 + (1 - \overline{R}_\rho)K'_S/K_S]s[\varepsilon_x - s(1 + \varepsilon_z)]$$
$$- \gamma'_{\text{eff}} s(\varepsilon_x - s\varepsilon_z)/\varepsilon_z\} = 0. \qquad (13)$$

Thus, either $m^2 = 0$ or the expression in braces is zero. In the latter case the equality can be written

$$\frac{(s-a)^2}{a^2} + \frac{(m^2)^2}{b^2} = 1, \qquad (14)$$

where

$$a = \frac{\varepsilon_x}{2} \frac{\gamma'_{\text{eff}}/\varepsilon_z + 1 + (1-\overline{R}_\rho)K'_S/K_S}{\gamma'_{\text{eff}} + [1 + (1-\overline{R}_\rho)K'_S/K_S](1+\varepsilon_z)}$$

$$b = \frac{\varepsilon_x}{2} \frac{\gamma'_{\text{eff}}/\varepsilon_z + 1 + (1-\overline{R}_\rho)K'_S/K_S}{[\gamma'_{\text{eff}}\,\text{Pr}\{\gamma'_{\text{eff}} + [1 + (1-\overline{R}_\rho)K'_S/K_S](1+\varepsilon_z)\}]^{1/2}}. \qquad (15)$$

If b is real (as for the constant γ_f case shown in Fig. 2), (14) describes an ellipse in the (s,m^2) plane; all values of s and m^2 within the ellipse correspond to exponentially growing solutions. If b is imaginary, the marginal stability curve is hyperbolic, and there is no high wavenumber cutoff for growth (this case will be discussed in section 4).

The real part of the growth rate is contoured in Fig. 3 as a function of the slope s and squared vertical wavenumber m^2 ($\overline{R}_\rho$ = 1.6, Pr = 5, $\mathcal{S}_x$ = 0.05, γ_f = 0.6, and K^t/K^f_S = 0.1). For each s and m^2, the root of (11) with the largest real part is shown. Shading shows growth rates with nonzero imaginary part, indicating solutions that oscillate as they grow or decay. The heavy line is the curve Re(λ) = 0; the ellipse described by (14) surrounds the region with positive, real growth rates. Growth rates for the oscillatory solutions depend strongly on m^2 and only weakly on s, indicating that these modes are strongly damped by friction.

3. The effect of turbulence

We first consider the case in which γ_f is constant but K^t is nonzero, in which case γ_{eff} increases monotonically with R_ρ, as shown in Fig. 2. Figure 4 shows the effect of nonzero K^t on the slope, wavenumber, and growth rate of the fastest-growing mode for the case Pr = 5, $\mathcal{S}_x$ = 0.05, as a function of R_ρ. The qualitative effect of turbulent mixing is to increase the vertical scale and decrease the slope and growth rate of the fastest-growing intrusions. The fastest-growing intrusion is quite sensitive to the turbulence level, especially for larger R_ρ.

a. Constant flux ratio case

If there is no turbulent mixing of T or S (K^t = 0) and if γ_f is constant, then (7) shows that γ_{eff} is also constant, and the problem reduces to the constant flux ratio case considered by Toole and Georgi (1981) and others. Growth rates for this case are contoured in Fig. 5. The appropriate limiting case of (15) is obtained by letting $\gamma'_{\text{eff}} \to 0$ in (15) and setting $\gamma_{\text{eff}} = \gamma_f$, giving

$$a = \frac{(1-\gamma_f)\mathcal{S}_x}{2(1 + (1-\gamma_f)\mathcal{S}_z)} \qquad b \to \infty, \qquad (16)$$

or equivalently

$$0 < s < \frac{(1-\gamma_f)\mathcal{S}_x}{1 + (1-\gamma_f)\mathcal{S}_z}. \qquad (17)$$

This range of slopes and wavenumbers corresponds to the shaded band in Fig. 6. The range of slopes is larger than for the case with nonzero K^t, and there is no high wavenumber cutoff for intrusion growth. The result (16) is independent of the value of the viscosity; changing the Prandtl number changes growth rates, but the shape of the marginal stability curve remains the same.

b. The limit of strong turbulent mixing

In this section, we will show that intrusions can grow even when turbulent fluxes of T and S are much larger than double-diffusive fluxes. If $K^f_S \sim K'^f_S \ll K^t$ and $\gamma'_f = 0$, then the semimajor axes (15) are approximated by

$$b = \frac{1}{2\ \mathrm{Pr}^{1/2}}(1 - \gamma_f)S_x\frac{K_S^f}{K^t}(\overline{R}_\rho + (\overline{R}_\rho - 1)^2 K_S'^f/K_S^f) + O([K_S^f/K^t]^2). \quad (18b)$$

Both axes (18a,b) are proportional to K^f_S/K^t if $K^f_S/K^t \ll 1$, implying that, for *any* finite value of K^f_S/K^t, there exists a finite area of the (s,m^2) plane in which intrusions can grow.[1] This suggests intrusions can grow even where double-diffusive fluxes are considerably smaller than turbulent fluxes, a rather surprising result. In the strong turbulence limit, (8) shows that the effective flux ratio is given by $\gamma_{\mathrm{eff}} = \overline{R}_\rho + O(K^f_S/K^t)$, which is larger than one for finger-sense stratification. In this case, the effective diffusivity for density is [from (9b,c)] $K_\rho = -K_S(1 - \gamma_{\mathrm{eff}})/(R_\rho - 1)$, which is positive, so the net buoyancy flux is downgradient (i.e., turbulent buoyancy fluxes dominate over double-diffusive fluxes). Double diffusion is characterized by upgradient buoyancy fluxes, so light water is made lighter and dense water denser; this mechanism is fundamental to intrusion growth, so it seems intuitive that intrusions should not grow when $\gamma_{\mathrm{eff}} > 1$. However, it is the ratio of T and S divergences— not the flux ratio— must be less than one to drive intrusion growth, and intrusions grow if this “flux divergence ratio,” $\Gamma_{\mathrm{div}} \equiv \alpha F_{T,z}/\beta F_{S,z}$, is less than one [Walsh and Ruddick (1998) discuss this point in some detail]. In the constant γ_f case with no turbulent mixing considered by Toole and Georgi (1981) and others, γ_f and Γ_{div} are exactly equal, making the distinction unnecessary. However, in the present case, an R_ρ-dependent flux ratio allows the flux divergence ratio to differ from the flux ratio (i.e., $\alpha F_{T,z}/\beta F_{S,z} = \gamma_{\mathrm{eff}} + \gamma'_{\mathrm{eff}} R_{\rho,z} F_S/F_{S,z} \neq \gamma_{\mathrm{eff}}$) so that intrusions may grow even when γ_{eff} is larger than one, as long as $\Gamma_{\mathrm{div}} < 1$.

c. The high-wavenumber cutoff

Figure 6 shows marginal stability curves for various values of K^t/K^f_S (numbers on the curves show the value of K^t/K^f_S). Increasing K^t/K^f_S causes the curve to move toward lower slopes and wavenumbers. Comparing these curves with the $K^t/K^f_S = 0$ case (shaded) shows that a major effect of turbulence is to stabilize high wavenumber disturbances. To explore the mechanism behind this, we compute eigenvectors for the system (10) in the large-m limit. For maximum simplicity, we consider the large Prandtl number limit, which is equivalent to assuming a steady momentum balance in (10a), allowing (10b,c) to be written as a closed set for $\tilde{S}$ and $\tilde{T}$. Assuming harmonic solutions gives

$$\lambda_* \beta\hat{S} + \frac{gk_*(\beta\hat{S} - \alpha\hat{T})}{Am_*^4}\beta(m_*\overline{S}_x - k_*\overline{S}_z) = -m_*^2([K_S - \overline{R}_\rho K_S']\beta\hat{S} + K_S'\alpha\hat{T}) \quad (19a)$$

$$\lambda_* \alpha\hat{T} + \frac{gk_*(\beta\hat{S} - \alpha\hat{T})}{Am_*^4}\alpha(m_*\overline{T}_x - k_*\overline{T}_z) = -m_*^2[\gamma_{\mathrm{eff}}(K_S - \overline{R}_\rho K_S') - \gamma'_{\mathrm{eff}}\overline{R}_\rho K_S]\beta\hat{S} - m_*^2[\gamma_{\mathrm{eff}}K_S' + \gamma'_{\mathrm{eff}}K_S]\alpha\hat{T}, \quad (19b)$$

(Click the equation graphic to enlarge/reduce size)

where $\hat{S}$ and $\hat{T}$ are the disturbance amplitudes. Because we are interested in exploring the high-wavenumber cutoff, which is not dependent on diffusivity variations, it is sufficient to consider the case $K'_S = 0$. In this case, (19a) gives

$$\frac{\beta\hat{S}}{\alpha\hat{T}} = \frac{\dfrac{gk_*}{Am_*^4}(m_*\overline{S}_x - k_*\overline{S}_z)}{\lambda_* + \dfrac{gk_*}{Am_*^4}(m_*\overline{S}_x - k_*\overline{S}_z) + m_*^2 K_S}. \quad (20)$$

In the large-m_* limit, the eigenvalues of (19) are $\lambda_* = -m^2{}_* K_S + O(m^{-4}{}_*)$ and $\lambda_* = -\gamma'_{\mathrm{eff}} m^2{}_* K_S + O(m^{-4}{}_*)$. We will consider the eigenvalue proportional to γ'_{eff}, since (15b) shows that a finite high-wavenumber cutoff requires that γ'_{eff} be positive. In the large-m_* limit, this eigenvalue corresponds to the eigenvector

$$\frac{\beta\hat{S}}{\alpha\hat{T}} = O(m_*^{-5}) \to 0, \qquad m_* \to \infty, \quad (21)$$

in which case the velocity $\hat{u} = gk^*(\beta\hat{S} - \alpha\hat{T})/Am^4{}_*$ also vanishes, so these modes are nonadvective in the limit as $m_* \to \infty$. For disturbances described by (21) Eqs. (19a,b) decouple, and (19b) shows that high wavenumber disturbances evolve according to a diffusion equation:

$$\alpha\tilde{T}_t = +\gamma'_{\mathrm{eff}} K_S \alpha\tilde{T}_{zz}. \quad (22)$$

If $\gamma'_{\mathrm{eff}} > 0$, the effective diffusivity is positive, so disturbances decay.

d. The "incomplete" turbulent mixing case

The growth rate polynomial (11) is quite general, and growth rates for a wide variety of diffusivity and flux ratio formulations can be obtained as special cases of this polynomial. One such case is that considered by Hebert (1999), who proposed differential mixing of T and S due to low-Reynolds-number turbulence as a possible driving mechanism for intrusions. The idea of differential mixing originated in laboratory experiments done by Turner (1965), who measured turbulent fluxes across a density interface as a function of interfacial Reynolds number. Turner found larger effective diffusivities when the stratification was maintained by temperature than for the salt stratification case. The differences were most pronounced at low Reynolds number, and Turner suggested that his results were a consequence of molecular modification of low-Reynolds-number turbulence. Based on Turner's results, Hebert assumed unequal, constant, diffusivities for T and S. This case can be recovered from our analysis by setting $\gamma_{\text{eff}} = \tau R_\rho$, where τ is a diffusivity ratio. This transforms (11) into the growth rate polynomial derived by Hebert (1999) for the &ldquo∞complete" turbulent mixing case. Equation (15) shows that, if $K^{f'}_S = 0$, then, if $\tau < 1$, the marginal stability curve is elliptical and solutions resemble intrusions, while, if $\tau > 1$, the marginal stability curve is hyperbolic and steeply sloped disturbances reminiscent of salt fingers grow.

4. Double-diffusive effects: The form of the salt finger flux ratio

We next consider the purely double-diffusive case and the effect of using a variable finger flux ratio γ_f. There are a variety of theoretical possibilities for the flux ratio. Stern (1975, section 11.2) considers the stability of uniform finger-sense gradients to vertically oriented finger motions sinusoidal in x and y. He solves for the maximum growth rate in the limit of large Prandtl number and diffusivity ratio, and finds the following form for the finger flux ratio:

$$\gamma_f(R_\rho) = R_\rho - \sqrt{R_\rho(R_\rho - 1)}, \qquad (23)$$

which is shown as a solid curve in Fig. 7. This functional form decreases monotonically with R_ρ from a value of 1 at $R_\rho = 1$ to below 0.6 at $R_\rho = 2$ and asymptotes to 0.5 at large R_ρ. This form is also found by the finger model of Kunze (1987). Schmitt (1979a) extended Stern's model to finite Prandtl number and diffusivity ratios, solved indirectly for the fastest-growing mode, and found a closed but rather complicated form for the finger flux ratio. Schmitt's flux ratio decreases from ≈0.74 at $R_\rho = 1$ to a minimum of ≈0.56 at $R_\rho \approx 4$, and then begins to increase slowly (dashed curve in Fig. 7), asymptoting to $(R_\rho/\tau)^{1/2}$ for large R_ρ (τ is the diffusivity ratio). Schmitt also postulated a physically appealing interface model in which initial gradients set the fastest-growing wavelength, but fluxes eventually decrease the salinity gradient in the interior of the interface to allow fingers to equilibrate. The associated flux ratio for this equilibrium state is slightly higher than Schmitt's fastest-growing form but has qualitatively similar characteristics and the same asymptote at high R_ρ.

The three flux ratio formulations all have similar characteristics and values for the range $R_\rho \lesssim 4$, where fingers might dominate over turbulence. In the range $4 \lesssim R_\rho \lesssim 10$, the Schmitt formulation has positive slope while Stern's has negative slope, but quantitative differences between the three are small. The scatter and range of observed flux ratios from laboratory experiments is too large to allow one formulation to be selected over others. The main characteristic that laboratory experiments demonstrate is a systematic increase in flux ratio as R_ρ approaches 1, and all three formulas capture this characteristic. Nevertheless, the relatively small differences between the these formulations lead to important differences in the behavior of our model solutions. We have chosen to use Stern's flux ratio (23) and Schmitt's fastest-growing finger formulation [Eq. (12) from Schmitt (1979a)] to illustrate these differences.

a. UV catastrophe

In this section, we demonstrate that the flux ratio (23) and that proposed by Schmitt (1979a) lead to a "UV catastrophe" in which growth rates increase monotonically with vertical wavenumber m (see Fig. 8) and become unbounded as $m \to \infty$. To examine the effect in the simplest way possible, we first show that the instability occurs in a simplified nonadvective system, then show that it also occurs in the full interleaving system. For maximum simplicity, we replace K_S by K^f_S (so vertical fluxes are purely double diffusive) and γ_{eff} in (10) by either Stern's (1975) formulation (23) or by Schmitt's (1979a) formulation, and consider the limiting case in which advective effects are negligible. This gives

$$\beta\tilde{S}_t = [K^f_S - \overline{R}_\rho K^{f'}_S]\beta\tilde{S}_{zz} + K^{f'}_S \alpha\tilde{T}_{zz} \qquad (24a)$$

$$\alpha\tilde{T}_t = [\gamma_f(K^f_S - \overline{R}_\rho K^{f'}_S) - \gamma'_f \overline{R}_\rho K^f_S]\beta\tilde{S}_{zz} + [\gamma_f K^{f'}_S + \gamma'_f K^f_S]\alpha\tilde{T}_{zz}, \qquad (24b)$$

which is very similar to the system analyzed by Walsh and Ruddick (1995b), except that here we allow for a nonconstant flux ratio.

The characteristic polynomial for (24) is

$$= 0. \qquad (25)$$

There are positive roots (i.e., growing solutions) to (25) when the braced term is negative (i.e., $\gamma'_f < 0$). Because γ'_f is always negative for Stern's formulation (23), there is always one positive real (growing) root and one negative real (decaying) root to (25), regardless of the sign or magnitude of $K^{f'}_S/K^f_S$. If $K^{f'}_S/K^f_S$ is negligible, the roots of (25) are

$$\lambda = -m^2 \quad \text{or} \quad \lambda = -\gamma'_f m^2, \qquad (26)$$

the second of which is the unstable root. Hence, using Stern's formulation (23) for the flux ratio changes the marginally stable root ($\lambda = 0$) found by Walsh and Ruddick (1995b) to an unstable root; Schmitt's formulation has the same effect for $R_\rho \lesssim 4$. Any negative value of γ'_f, however small, is sufficient to trigger the UV catastrophe. Equation (26) implies that $\lambda \to \infty$ as $m^2 \to \infty$: there is no upper bound to the growth rate. In reality this cannot be strictly true since small-scale dissipative effects will act to suppress the highest wavenumber disturbances. In addition, it is worth noting that our parameterization of salt finger fluxes cannot in any case be valid at scales smaller than the salt finger scale.

Equations (24) and (26) show that the UV instability does not rely on lateral advection, and hence is not intrusive in nature. Furthermore, the instability is different from the high-wavenumber intrusive instability found by Stern (1967) because it is nonadvective (and hence cannot be suppressed by friction). Instead, it is closely related to that discussed by Huppert (1971), who considered a system of three fluid layers separated by diffusive interfaces and found that layer overturning occurred when the flux ratio decreased with R_ρ. In contrast with Huppert's study, where a layer scale was imposed, there is no external length scale in this study, so arbitrarily small scales can grow. Comparison of (24) with (19) shows that (24) is the high-wavenumber limit of the full system (with $K^t = 0$), demonstrating that diffusion dominates over advection at high wavenumber and that high wavenumber solutions to the full interleaving system (10) should be well described by (24).

To illustrate the mechanism for the UV instability, we compute eigenvectors of the system (24). Equation (24a) gives

$$\frac{\beta\hat{S}}{\alpha\hat{T}} = \frac{-m^2 K^{f'}_S/K^f_S}{\lambda + m^2(K^f_S - \overline{R}_\rho K^{f'}_S)/K^f_S}, \qquad (27)$$

where $\hat{S}$ and $\hat{T}$ are disturbance amplitudes. We set $K^{f'}_S = 0$ without (much) loss of generality since (25) shows that the instability does not require variations in K^f_S. Substituting the unstable eigenvalue ($\lambda = -\gamma'_f m^2$) into (27) gives

$$\frac{\beta\hat{S}}{\alpha\hat{T}} = 0, \qquad (28)$$

in which case (24a,b) decouple, and (24b) shows that the disturbance evolves according to

$$\alpha\tilde{T}_t \approx +\gamma'_f K^f_S \alpha\tilde{T}_{zz}. \qquad (29)$$

Because $\gamma'_f < 0$, the effective diffusivity is negative, so disturbances grow.

The instability mechanism is sketched in Fig. 9. The basic state has uniform vertical T–S gradients and uniform vertical fluxes. A small T disturbance (leftmost profile) produces a corresponding R_ρ disturbance, and because γ_f is a decreasing function of R_ρ the flux ratio varies as shown. Salt fluxes are unaffected by the imposed temperature anomaly, and because fluxes of T and S are linked via (4) the heat flux at **A** increases relative to that at **B** (as shown in the rightmost profile), reinforcing the initial perturbation and causing growth. The equations governing the growth of the instability can also be derived directly from the temperature equation as follows:

$$\alpha\tilde{T}_t = (\gamma_f \beta K^f_S S_z)_z = \gamma'_f(\overline{R}_\rho)R_{\rho z}\beta K^f_S \overline{S}_z = \gamma'_f K^f_S \alpha\tilde{T}_{zz},$$
$$(K^f_S = \text{const}, \tilde{S} = 0) \qquad (30)$$

in agreement with (29).

b. Turbulent suppression of the UV catastrophe in the reduced system

The discussion in section 4a related the UV catastrophe to the form of the flux ratio for the system (24). This is readily generalized to give a stability criterion when turbulent mixing of T and S is present:

$$\frac{\partial \gamma_{\text{eff}}}{\partial R_\rho} > 0 \qquad (31)$$

is sufficient to prevent the UV catastrophe &lsqb is follows directly from (22)]. In Fig. 10, γ_{eff} is plotted versus R_ρ for various values of K^t, using Stern's γ_f formulation (23) (Fig. 10a); in Fig. 10b the same quantities are plotted for Schmitt's (1979a) formulation. For the Stern formulation, there is always a range of R_ρ in which $\gamma'_{\text{eff}} < 0$ while, for sufficiently large R_ρ, $\gamma'_{\text{eff}} > 0$ for any nonzero K^t. Further, for any value of K^t, we are assured that γ'_{eff} will be negative for sufficiently small R_ρ since $\gamma'_f \rightarrow -\infty$ as $R_\rho \rightarrow 1$ for Stern's formula. The dashed curve in Fig. 10a is the function $R_\rho/(2R_\rho - 1)$, which connects the minima of the solid curves. Points beneath this curve are unstable to the UV instability, those above it are stable. Thus, *T*–*S* profiles subject to Stern's flux ratio with an effective *T*/*S* flux ratio less than $R_\rho/(2R_\rho - 1)$ will be unstable to the UV instability—a result which holds for any value of K^t. Figure 10b is similar to Fig. 10a except quantities are plotted using Schmitt's flux ratio instead of Stern's. The two plots are similar in many respects, but in Fig. 10b there is a critical value of K^t/K^f_S above which γ_{eff} increases monotonically for all values of R_ρ (a consequence of the finite slope of Schmitt's curve as $R_\rho \rightarrow 1$). Thus, for Schmitt's γ_f formulation, sufficiently large values of K^t/K^f_S ($K^t/K^f_S \gtrsim 0.59$) will suppress the high-wavenumber instability for all R_ρ. Furthermore, since $\gamma'_f > 0$ for Schmitt's formulation whenever $R_\rho \gtrsim 4$, the UV instability will be suppressed even in the absence of background turbulence for large R_ρ.

Using the definition of γ_{eff} (8), the above stability condition (31) can be written as a constraint on K^t:

$$\frac{K^t}{K^f_S}\left[1 + (\gamma_f - \bar{R}_\rho)\frac{K^{f'}_S/K^f_S}{1 + K^t/K^f_S}\right] > -\gamma'_f \qquad (32)$$

and, if terms involving $K^{f'}_S$ are negligible, this takes the simple form

$$\frac{K^t}{K^f_S} > -\gamma'_f \qquad (33)$$

as the condition to suppress the UV instability. When $\gamma'_f < 0$, a nonzero K^t is required to suppress the instability, and it follows that when $K^t = 0$ instabilities grow for *any* negative γ'_f. Neglect of terms involving $K^{f'}_S$ in (33) is not equivalent to assuming that K^f_S is strictly constant, but rather that variations in K^f_S associated with small amplitude intrusions are not of *O* (1) importance. Nevertheless, (32) shows that sufficiently large, positive values of $K^{f'}_S$ &lsqb≲ke those predicted by Kunze's (1987) salt finger model] could have a destabilizing effect. Substitution of Kunze's (1987) formulation for K^f_S into (32) (and using Stern's flux ratio) shows that a nearly uniform value of 3–4 ($\times 10^{-6}$ m^2 s^{-1}) for K^t is sufficient to suppress the UV instability, except at very small values of R_ρ ($R_\rho \lesssim 1.2$) where K^t values of up to 2–3 ($\times 10^{-5}$ m^2 s^{-1}) are needed. Using Schmitt's flux ratio gives similar results, although somewhat smaller values (about 25%– 50% smaller for R_ρ values between 1 and 3) of K^t are needed to suppress the instability. By contrast, Fig. 11 shows that when $K^t \approx$ 3–4 ($\times 10^{-6}$ m^2 s^{-1}) and $R_\rho \approx 2$, K^f_S must be larger than about 5×10^{-5} m^2 s^{-1} to trigger the UV instability, much larger than the analogous value of about 1×10^{-5} m^2 s^{-1} required when Kunze's diffusivity is used.

Violation of the criterion (33) could lead to growth of high-wavenumber instabilities, and it is plausible that this is related to the "steppy" finestructure often seen at low values of R_ρ, where double diffusion may dominate over turbulence. The quantity $-1/\gamma'_f$ is plotted in Fig. 11 for both the Stern (solid) and Schmitt (dashed) flux ratio formulations. According to (33), *y*-axis values represent critical values of K^f_S/K^t below which the UV instability is suppressed. For larger values of R_ρ, larger finger diffusivities are required to trigger the UV instability. Using Stern's formulation, and assuming that $K^t = 10^{-5}$ m^2 s^{-1}, it follows that K^f_S must be at least 4×10^{-5} m^2 s^{-1} to cause instability when $R_\rho \approx 1.5$, but must be greater than the (very large) value of 5×10^{-4} m^2 s^{-1} for the instability to occur when $R_\rho \approx 3$. Schmitt's γ_f formulation is &ldquo≷re stable" than Stern's, since larger values of K^f_S/K^t are required to trigger the UV instability for all values of R_ρ.

c. Generalization to the full interleaving system

Equation (22) from section 3c and the discussion in section 4b shows that a sufficient condition for the occurrence of the UV instability in the reduced (nonadvective) system is that γ_{eff} be a decreasing function of R_ρ; that is,

$$\gamma'_{\text{eff}} < 0. \qquad (34)$$

Thus, the sign of γ'_{eff} is fundamental to the behavior of the system (10): when $\gamma'_{\text{eff}} \leq 0$ there is no high-wavenumber cutoff, so disturbances of arbitrarily small scale can grow. Similarly, expansion of (11) shows that there are solutions to (11) of the form

$$\lambda/m^2 = -\gamma'_{\text{eff}}/[1 + (\gamma_{\text{eff}} - \overline{R}_\rho)K'_S/K_S] + O(\gamma'_{\text{eff}})$$

in the high-wavenumber limit, valid when $\gamma'_{\text{eff}} \ll 1$. This demonstrates again that the full interleaving system (10) is susceptible to the UV instability when $\gamma'_{\text{eff}} < 0$. In contrast with (34), (15b) shows that there is no high-wavenumber cutoff when

$$\gamma'_{\text{eff}}\,\text{Pr}\left\{\gamma'_{\text{eff}} + [1 + (1 - \overline{R}_\rho)K'_S/K_S]\frac{\overline{R}_\rho - \gamma_{\text{eff}}}{\overline{R}_\rho - 1}\right\} \leq 0, \qquad (35)$$

and the marginal stability curve is hyperbolic when this inequality is satisfied. In the appendix, we show that the quantity in braces is positive for all $\overline{R}_\rho > 1$ for any of the the flux ratio formulations used in this study, so the sign of γ'_{eff} is sufficient to determine if (35) is satisfied.

Figure 12 shows the effect on the marginal stability curve of increasing K^t/K^f_S. For small values, the marginal stability curve is hyperbolic, with slopes and wavenumbers above the curve being unstable. Increasing K^t/K^f_S causes the curve to become elliptical when (33) is satisfied, and intrusions grow over the range of slopes and wavenumbers within the ellipse. The maximum growth rate is contoured in Fig. 13 for the case Pr = 5, $\overline{R}_\rho = 1.6$, $\mathcal{S}_x = 0.05$, $K^t/K^f_S = 0.1$, using Stern's flux ratio formulation (23). Intrusive disturbances dominate at low wavenumbers (as shown by the local growth rate maximum at small values of m^2), while growth rates increase monotonically for large m^2, where the high-wavenumber instability dominates. Note the spectral gap between intrusions and the high-wavenumber UV modes. In this case, the addition of turbulence has inhibited the UV instability, so intrusions are able to dominate at low wavenumbers. This is in contrast with Fig. 8, where the UV instability dominates for all values of s and m^2.

5. Discussion

The previous sections demonstrated that the system (10) is unstable to two different instabilities: an intrusive instability relying on buoyancy-driven advection across a front and a nonadvective "Huppert" instability resulting from the specific character of the vertical fluxes of T and S. Being predominantly a vertical process, the Huppert instability should have a preferred direction in T–S space distinct from that of intrusions, so the two phenomena should be distinguishable in T–S data. Specifically, intrusions (which are nearly isopycnal advective features) should cause zigzags in the T–S curve that are nearly aligned with density lines, while the high-wavenumber (UV) instability should cause "bunching" along the T–S curve. It is possible that the UV instability considered here is related to the formation of the steps and layers often seen at low R_ρ. Unfortunately, our analysis does not allow a prediction of the dominant scale of steppy finestructure, which might result from the UV instability, since the scale-selection mechanism at work in the ocean almost certainly relies on small-scale physics not contained in our model.

If something akin to the UV instability does occur in the ocean and if it leads to the formation of steps and layers, then the vertical fluxes of heat and salt driving intrusion growth would very likely change as well. This potential for modification of vertical fluxes by high-wavenumber instabilities and the consequent modification of intrusion growth rates suggests a possible interaction between instability modes that cannot be studied within the context of our model. Nevertheless, many of the qualitative features of our analysis should still hold. It is possible that a similar combination of high-wavenumber instabilities and low-wavenumber intrusive instabilities could explain observations of steppy intrusions made by Perkin and Lewis (1984).

While we have not discussed the effect of R_ρ-dependent diffusivities in detail, we feel that these effects are not likely to qualitatively change the conclusions of this work. This does not imply, however, that an R_ρ-dependent diffusivity cannot have important qualitative effects on oceanic processes in other circumstances; Schmitt (1981) argues that an R_ρ-dependent diffusivity may provide the mechanism for maintaining the nearly uniform values of R_ρ in the central waters. And there are several ways in which an R_ρ-dependent diffusivity could quantitatively affect our results, the most obvious being through changing the properties of the marginal stability curve. For example, Walsh and Ruddick (1995a) carried out a detailed analysis of the effect of diffusivities that are decreasing functions of R_ρ (like that proposed by Schmitt 1981) on small amplitude interleaving, finding enhanced growth rates and larger vertical scales for the fastest-growing intrusions.

On a more qualitative level, a nonconstant diffusivity could allow different types of instabilities to occur. Walsh and Ruddick (1995b) discussed instabilities resulting from the salt-finger diffusivity parameterizations due to Stern (1969) and Kunze (1987). These authors proposed flux-limiting constraints for growing salt fingers, resulting in diffusivity formulations which are increasing functions of R_ρ. Walsh and Ruddick (1995b) showed that diffusivities of this form can lead to a UV

catastrophe if they are rapidly increasing functions of R_ρ because the effective diffusivity for T–S anomalies [$K^f_S + (\gamma_f - \overline{R}_\rho) K^{f'}_S$] can then be negative. The instability that occurs in this case is similar to that discussed by Phillips (1972). The Phillips instability occurs when the flux of a quantity Φ decreases as its gradient is increased. Hence, if the vertical flux of Φ is characterized by a nonlinear diffusivity so that the flux $F_{(\Phi)}$ is given by

$$F_{(\Phi)} = -K(\Phi_z)\Phi_z, \quad (36)$$

small perturbations will grow if the "effective diffusivity" is negative, that is,

$$\frac{\partial}{\partial \phi_z}(K(\phi_z)\phi_z) < 0. \quad (37)$$

This condition is satisfied if $K(\Phi_z)$ decreases faster than Φ^{-1}_z, in which case the flux of Φ increases where gradients are weak and decreases where they are large, causing disturbances to grow. In our case the situation is slightly different because the flux of salt is given by $F_S = -K_S(R_\rho)S_z$ [according to (6)], and R_ρ has an inverse dependence on S_z [from (5)]. It follows that, for fixed T_z, instability will occur if K_S increases faster than linearly (i.e., faster than R^{+1}_ρ). Such behavior could affect our conclusions significantly if it occurred, although the growth rate expression (11) and the expressions for the marginal-stability curve [(14), (15)] would still be valid. However, evidence suggests that effective diffusivities in salt-finger-stratified regions of the ocean are decreasing functions of R_ρ (Schmitt 1981) [except perhaps at rather low values of R_ρ (Kunze 1994)], in which case the instability discussed by Walsh and Ruddick (1995b) would not occur. In contrast, evidence that the flux ratio decreases with R_ρ seems stronger [e.g., Schmitt (1979b); St. Laurent and Schmitt (1999)], so the "Huppert" instability discussed in this work may be more relevant to the ocean.

A better understanding of the large amplitude behavior of thermohaline interleaving is needed to evaluate its role in the ocean. To achieve this, an improved understanding of the small-scale fluxes driving intrusions is needed, as is a better understanding of the ways interleaving structures interact with the mesoscale features in which they are embedded. Our approach in this work has been to examine the effect of particular assumptions about small-scale double-diffusive and turbulent fluxes on small amplitude intrusions. Eventually, we hope to be able to reliably predict the fluxes of heat, salt, density, and momentum associated with fully developed interleaving for any particular set of initial conditions (e.g., stratification, lateral T–S gradients, shear). This will require an understanding of the large amplitude dynamics of intrusions, and at present we are a long way from having the necessary level of understanding. Some progress in this direction has been made by McDougall (1985b), who obtained a family of equilibrium solutions representing large amplitude, &ldquo~ ab" intrusions (i.e., convecting layers separated by thin diffusive and salt finger interfaces) and analyzed their stability in a heuristic fashion. Walsh and Ruddick (1998) used a one-dimensional numerical model to show how the fluxes of T and S driving intrusions can adjust as they grow to allow small-amplitude, exponentially growing intrusions to achieve a large amplitude equilibrium. Recently, Merryfield (2000) has presented model results suggesting that intrusions may in some cases evolve into thermohaline staircases, rather than the large amplitude equilibrium intrusions found by Walsh and Ruddick (1998). This remains an active area of investigation.

6. Conclusions

The interleaving problem has been formulated such that the combined effects of turbulence and double diffusion are characterized by an R_ρ-dependent flux ratio, γ_{eff}. This approach allows the two phenomena to be studied and compared within the same theoretical framework. Turbulence decreases the range of slopes and wavenumbers over which intrusions grow, but intrusions still grow for any finite value of K^t/K^f_S. This suggests that interleaving can occur even when turbulent fluxes are larger than double-diffusive fluxes, as may be the case over much of the world's ocean.

The qualitative behavior of the interleaving system (10) is found to depend upon the variation of γ_{eff} with R_ρ: when $\gamma'_{\text{eff}} > 0$ (the &ldquo▲rbulence-dominated" case), the marginal stability curve is elliptical and high-wavenumber disturbances are suppressed; when $\gamma'_{\text{eff}} < 0$ (the "finger-dominant" case) the marginal stability curve is hyperbolic and growth rates are unbounded as $m \to \infty$. The expression (14) describing the marginal stability curve is very general, giving qualitative information about the stability of the system (10) independent of the detailed form of K^f_S and γ_f.

A nonconstant salt-finger flux ratio that is a decreasing function of R_ρ (Stern 1975; Schmitt 1979a) leads to a UV catastrophe, the mechanics of which are similar to that for the instability discussed by Huppert (1971). This UV instability is nonadvective in the large m limit and hence cannot be suppressed by friction, in contrast with the high-wavenumber intrusive instability discussed by Stern (1967). However, in most cases, the UV instability can be suppressed by turbulent mixing of T and S, and we present a simple criterion for this, relating the strength of turbulence to double diffusion. For Stern's formulation (23) the high-wavenumber instability occurs for small enough R_ρ for any K^t/K^f_S, whereas for Schmitt's formulation values of K^t/K^f_S larger than ≈ 0.59 will suppress the high wavenumber instability for all R_ρ. Even when the UV instability occurs, the fastest-growing low-wavenumber disturbances may still be intrusive for moderate turbulence levels. The spectral gap between intrusions at low-wavenumber and high-wavenumber UV modes may help explain observations of intrusions in a background of smaller-scale steps and layers (e.g., Perkin and Lewis 1984).

Acknowledgments

We wish to acknowledge helpful comments made by Ray Schmitt, as well as a very detailed and helpful review by Eric Kunze.

REFERENCES

Barton, E. D., and P. Hughes, 1982: Variability of water mass interleaving off N.W. Africa. *J. Mar. Res.,* **40,** 963–984.

Carmack, E. C., K. Aagaard, J. H. Swift, R. G. Perkin, F. A. McLaughlin, R. W. Macdonald, and E. P. Jones, 1998: Thermohaline transitions. *Physical Processes in Lakes and Oceans,* J. Imberger, Ed., Vol. 54, Coastal and Estuarine Studies, Amer. Geophys. Union, 179–186.

Crapper, P. F., 1976: The transport across a density interface in the presence of externally imposed turbulence. *J. Phys. Oceanogr.,* **6,** 982–984.

Hamon, B. V., 1967: Medium-scale temperature and salinity structure in the upper 1500 m in the Indian Ocean. *Deep-Sea Res.,* **14,** 169–181.

Hebert, D., 1999: Intrusions: What drives them? *J. Phys. Oceanogr.,* **29,** 1382–1391.

Holyer, J. Y., 1983: Double-diffusive interleaving due to horizontal gradients. *J. Fluid Mech.,* **137,** 347–362.

Horne, E. P. W., 1978: Interleaving at the subsurface front in the slope water off Nova Scotia. *J. Geophys. Res.,* **83,** 3659–3671.

Huppert, H. E., 1971: On the stability of a series of double-diffusive layers. *Deep-Sea Res.,* **18,** 1005–1021.

Kelley, D., 1984: Effective diffusivities within oceanic thermohaline staircases. *J. Geophys. Res.,* **89,** 10484–10488.

Kunze, E., 1987: Limits on growing, finite-length salt fingers: A Richardson number constraint. *J. Mar. Res.,* **45,** 533–556.

— ,1994: A proposed flux constraint for salt fingers in shear. *J. Mar. Res.,* **52,** 999–1016.

Kuz'mina, N. P., and V. B. Rodionov, 1992: Influence of baroclinicity on formation of thermohaline intrusions in ocean frontal zones. *Izv. Atmos. Oceanic Phys.,* **28** (10–11), 804–810.

Ledwell, J. R., A. J. Watson, and C. S. Law, 1993: Evidence for slow mixing across the pycnocline from an open-ocean tracer-release experiment. *Nature,* **364,** 701–703.

Linden, P., 1971: Salt-fingers in the presence of grid-generated turbulence. *J. Fluid Mech.,* **49,** 611–624.

May, B. D., and D. E. Kelley, 1997: Effect of baroclinicity on double-diffusive interleaving. *J. Phys. Oceanogr.,* **27,** 1997–2008.

McDougall, T. J., 1985a: Double-diffusive interleaving. Part I: Linear stability analysis. *J. Phys. Oceanogr.,* **15,** 1532–1541.

— ,1985b: Double-diffusive interleaving. Part II: Finite amplitude, steady state interleaving. *J. Phys. Oceanogr.,* **15,** 1542–1556.

— ,and B. R. Ruddick, 1992: The use of ocean microstructure to quantify both turbulent mixing and salt fingering. *Deep-Sea Res.,* **39,** 1931–1952.

Merryfield, W. J., 2000: Origin of thermohaline staircases. *J. Phys. Oceanogr.,* **30,** 1046–1068.

Osborne, T. R., and C. S. Cox, 1972: Oceanic fine structure. *Geophys. Fluid Dyn.,* **3,** 321–345.

Perkin, R. G., and E. L. Lewis, 1984: Mixing in the West Spitsbergen Current. *J. Phys. Oceanogr.,* **14,** 1315–1325.

Phillips, O. M., 1972: Turbulence in a strongly stratified fluid—Is it unstable? *Deep-Sea Res.,* **19,** 79–81.

Richards, K. J., and R. T. Pollard, 1991: Structure of the upper ocean in the western equatorial Pacific. *Nature,* **350,** 48–50.

Ruddick, B. R., 1992: Intrusive mixing in a Mediterranean salt lens— Intrusion slopes and dynamical mechanism. *J. Phys. Oceanogr.,* **22,** 1274–1285.

— ,D. Walsh, and N. Oakey, 1997: Variations in apparent mixing efficiency in the North Atlantic central water. *J. Phys. Oceanogr.,* **27,** 2589–2605.

Schmitt, R. W., 1979a: The growth rate of super-critical salt fingers. *Deep-Sea Res.,* **26A,** 23–40.

— ,1979b: Flux measurements on salt fingers at an interface. *J. Mar. Res.,* **37,** 419–436.

— ,1981: Form of the temperature–salinity relationship in the central water: Evidence for double-diffusive mixing. *J. Phys. Oceanogr.,* **11,** 1015–1026.

— ,H. Perkins, J. D. Boyd, and M. C. Stalcup, 1987: An investigation of the thermohaline staircase in the western tropical North

Atlantic. *Deep-Sea Res.*, **34,** 1655–1666.

Stern, M. E., 1967: Lateral mixing of water masses. *Deep-Sea Res.*, **14,** 747–753.

— ,1969: Collective instability of salt fingers. *J. Fluid Mech.*, **35,** 209–218.

— ,1975: *Ocean Circulation Physics.* Academic Press, 246 pp.

St. Laurent, L., and R. W. Schmitt, 1999: The contribution of salt fingers to vertical mixing in the North Atlantic Tracer Release Experiment. *J. Phys. Oceanogr.*, **29,** 1404–1424.

Stommel, H., and N. K. Fedorov, 1967: Small scale structure in temperature and salinity near Timor and Mindinao. *Tellus*, **19,** 306– 325.

Toole, J. M., 1981: Intrusion characteristics in the Antarctic polar front. *J. Phys. Oceanogr.*, **11,** 780–793.

— ,and D. T. Georgi, 1981: On the dynamics and effects of double-diffusively driven intrusions. *Progress in Oceanography*, Vol. 10, Pergamon, 121–145.

Turner, J. S., 1965: The coupled turbulent transports of salt and heat across a sharp density interface. *Int. J. Heat Mass. Transfer*, **8,** 759–767.

— ,1973: *Buoyancy Effects in Fluids.* Cambridge University Press, 368 pp.

Walsh, D., and B. R. Ruddick, 1995a: Double-diffusive interleaving:The influence of non-constant diffusivities. *J. Phys. Oceanogr.*, **25,** 348–358.

— ,and — ,1995b: An investigation of Kunze's salt finger flux laws—Are they stable? *Double-Diffusive Convection, Geophys. Monogr.*, No. 94, Amer. Geophys. Union, 334 pp.

— ,and — ,1998: Nonlinear equilibration of thermohaline intrusions. *J. Phys. Oceanogr.*, **28,** 1043–1070.

APPENDIX

7. Determination of Sign of Coefficient in Eq. (35)

We want to demonstrate that

$$\gamma'_{\text{eff}} + (1 + (1 - \overline{R})K'_S/K^f_S)\frac{\overline{R}_\rho - \gamma_{\text{eff}}}{\overline{R}_\rho - 1} > 0. \quad \text{(A1)}$$

Using (8) and assuming $K'_S = 0$, this reduces to

$$(K^t/K^f_S + \gamma'_f) + \frac{\overline{R}_\rho - \gamma_f}{\overline{R}_\rho - 1} > 0. \quad \text{(A2)}$$

We will show that this inequality is satisfied for any of the flux ratio formulations considered in this work so that the inequality (35) is fully determined by the sign of γ'_{eff}. Now, Eq. (A2) is clearly satisfied if γ_f is constant and less than one (since $\overline{R}_\rho \geq 1$). In addition, using Stern's formulation gives, after some manipulation:

$$(K^t/K^f_S + 1)\sqrt{\overline{R}_\rho(\overline{R}_\rho + 1)} + \frac{1}{2} > 0, \quad \text{(A3)}$$

which is always positive. From (A2) we can see the reason for this is that the singularity in Stern's formulation, which is of the form $\gamma'_f \sim (\overline{R}_\rho - 1)^{-1/2}$ is weaker than the $(\overline{R}_\rho - 1)^{-1}$ singularity in the last term on the left-hand side of (A2), so the latter term (which is positive) dominates as $\overline{R}_\rho \to 1$. Finally, plotting the left side of (A2) versus R_ρ for different values of K^t/K^f_S using Schmitt's formulation shows that the inequality (A2) is indeed satisfied for any of the flux ratio formulations considered in this work. Thus, the sign of γ'_{eff} is sufficient to determine whether the UV catastrophe will occur in the full interleaving system (10).

Figures

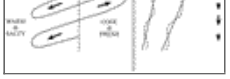

Click on thumbnail for full-sized image.

Fig. 1. Schematic of interleaving disturbances growing on a *T*–*S* front. Warm and salty water rises as it crosses the front; water from the cool, fresh side descends across the front. Lateral motions through horizontal *T*–*S* gradients produce small *T*–*S* disturbances (shown at right for the profile at location A), and the resultant variations in double-diffusive density fluxes (shown by arrows) accelerate the cross-front motion

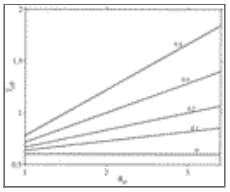

Click on thumbnail for full-sized image.

Fig. 2. Effect of turbulence on the effective *T*/*S* flux ratio γ_{eff} when γ_f is constant ($\gamma_f = 0.6$) (numbers on the curves show the value of K^t/K^f_S)

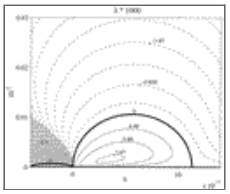

Click on thumbnail for full-sized image.

Fig. 3. Real part of growth rate contoured as a function of slope (*s*) and squared wavenumber (m^2) for the constant γ_f (=0.6) case with nonzero K^t ($K^t/K^f_S = 0.1$). Dashed contours show negative growth rates; shading indicates complex growth rates (i.e., oscillatory solutions). The heavy solid line shows the curve Re(λ) = 0

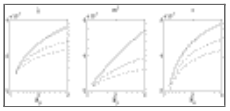

Click on thumbnail for full-sized image.

Fig. 4. Effect of turbulence on the properties of the fastest growing intrusion, plotted as a function of R_ρ for various values of K^t/K^f_S [$K^t/K^f_S = 0$ (solid), $K^t/K^f_S = 0.1$ (dashed), and $K^t/K^f_S = 0.2$ (dash-dotted)], with $\gamma_f = 0.6$, Pr = 5, $\mathcal{S}_x = 0.05$, and $K^{f'}_S/K^f_S = 0$

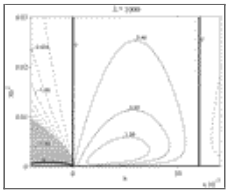

Click on thumbnail for full-sized image.

Fig. 5. As in Fig. 3 but with $K^t = 0$. In this case there is no high wavenumber cutoff for intrusion growth

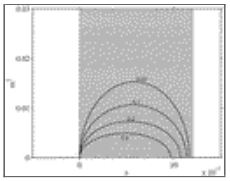

Click on thumbnail for full-sized image.

Fig. 6. Marginal stability curves for the constant flux ratio case ($\gamma_f = 0.6$) with turbulent mixing (Pr = 5, $\mathcal{S}_x = 0.05$, $\overline{R}_\rho = 1.6$). The shaded band is the region in which intrusions grow in the absence of turbulence. The marginal stability region is elliptical when K^t is nonzero, and increasing K^t shifts the curve toward smaller slopes and wavenumbers (numbers on the curves show the value of K^t/K^f_S)

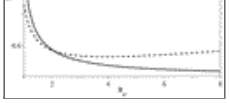

Click on thumbnail for full-sized image.

Fig. 7. Stern's (1975) salt finger flux ratio formula (23) (solid) and Schmitt's (1979a) formulation (dashed)

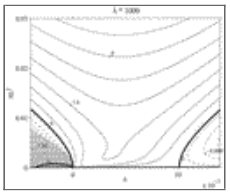

Click on thumbnail for full-sized image.

Fig. 8. Real part of growth rate contoured using Stern's flux ratio formulation (23), with $K^t = 0$, $\overline{R}_\rho = 1.6$, Pr = 5, and $\mathcal{S}_x = 0.05$. Largest wavenumbers grow fastest, and there is no local maxima corresponding to intrusions. Dashed contours show negative growth rates; shaded regions indicate oscillatory solutions. The heavy solid line shows the curve Re(λ) = 0

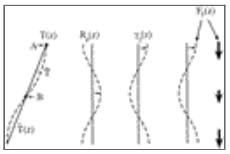

Click on thumbnail for full-sized image.

Fig. 9. Schematic of Huppert's (1971) instability mechanism. A small temperature disturbance produces a corresponding variation in R_ρ. If the flux ratio decreases with R_ρ this leads to vertical variations in the flux ratio as shown, and the resulting variations in the flux of T ($\alpha F_T = -\gamma_f \beta K^f{}_S \overline{S}_z$) cause the disturbance to grow

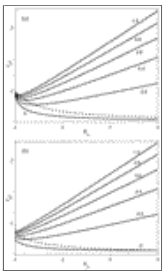

Click on thumbnail for full-sized image.

Fig. 10. Effect of turbulence on the effective flux ratio γ_{eff} using Stern's formulation for γ_f (a) and Schmitt's (1979a) formulation (b) for various values of $K^t/K^f{}_S$. Dashed curves connect the minima of the solid curves

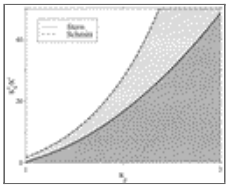

Click on thumbnail for full-sized image.

Fig. 11. Value of $K^f{}_S/K^t$ required to trigger the UV instability, as a function of R_ρ [from Eq. (33)]. Shaded regions are stable with respect to the high wavenumber UV instability discussed in the text. The dashed curve corresponds to Schmitt's (1979a) flux ratio formulation; the solid curve corresponds to Stern's formulation (23). When $R_\rho \approx 1$, relatively little double-diffusive mixing is needed to trigger the instability, but when R_ρ is large double diffusive fluxes must be very large to cause instability

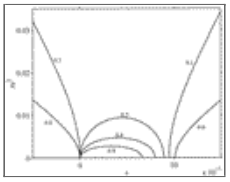

Click on thumbnail for full-sized image.

Fig. 12. Marginal stability curves using Stern's flux ratio formulation (23), for various values of $K^t/K^f{}_S$. The curves correspond

to the parameter choice Pr = 5, $\mathcal{S}_x$ = 0.05, $\overline{R}_\rho$ = 1.6, and the labels on the curves show the value of K^t/K^f_S. The marginal stability region is hyperbolic when K^t/K^f_S is small, and becomes elliptical when K^t/K^f_S exceeds the threshold defined by (33)

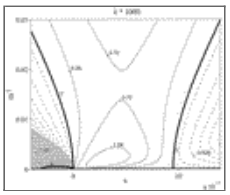

Click on thumbnail for full-sized image.

Fig. 13. Real part of growth rate contoured using Stern's flux ratio formulation (23) and nonzero K^t (K^t/K^f_S = 0.1); all other parameters are identical to those used in Fig. 8. As in Fig. 8, growth rates increase with m^2 for large m^2, suggesting a UV catastrophe, but the local maximum at $m^2 \approx 0.003$ shows that intrusions dominate at low wavenumbers. Dashed contours show negative growth rates, shaded areas show regions in which solutions are oscillatory, and the heavy solid line is the curve Re(λ) = 0

[1] Setting $\gamma'_f = 0$ has eliminated the high wavenumber instability, so all growing modes within the ellipse with semimajor axes (18a,b) must be intrusive in nature.

Corresponding author address: Dr. David Walsh, International Arctic Research Center, University of Alaska, Fairbanks, P.O. Box 757335, Fairbanks, AK 99775-7335.

E-mail: dwalsh@iarc.uaf.edu

top